Journal of Power Sources 196 (2011) 666–673

Contents lists available at ScienceDirect

Journal of Power Sources

journal homepage: www.elsevier.com/locate/jpowsour

Dealloyed binary PtM_3 (M = Cu, Co, Ni) and ternary $PtNi_3M$ (M = Cu, Co, Fe, Cr) electrocatalysts for the oxygen reduction reaction: Performance in polymer electrolyte membrane fuel cells

Prasanna Mani[a,b], Ratndeep Srivastava[a], Peter Strasser[c,d,*]

[a] Department of Chemical & Biomolecular Engineering, University of Houston, Houston, TX 77204, United States
[b] NRC Institute for Fuel Cell Innovation, Vancouver, B.C. V6T 1W5, Canada
[c] The Electrochemical Energy, Catalysis, and Materials Science Laboratory, Department of Chemistry, Chemical Engineering Division, Technical University Berlin, 10623 Berlin, Germany
[d] Ertl Center for Electrochemistry and Catalysis, Gwangju Institute of Science and Technology (GIST), Gwanju, South Korea

ARTICLE INFO

Article history:
Received 7 May 2010
Received in revised form 12 July 2010
Accepted 18 July 2010
Available online 27 July 2010

Keywords:
Dealloyed
Catalysts
Alloy
ORR
MEA

ABSTRACT

Dealloyed Pt bimetallic nanoparticles are highly active electrocatalysts for the electroreduction of molecular oxygen (ORR), the key barrier to more efficient polymer electrolyte membrane fuel cells (PEMFCs). Most previous studies of dealloyed Pt alloys focused on the structure and mechanism of dealloyed Pt–Cu bimetallic materials. Also, stability concerns related to Cu prompted the search for alternative non-noble metal components for dealloying.

Here, we report on a comparative study of dealloyed binary PtM_3 (M = Co, Cu, Ni) electrocatalyst for use in PEMFC cathodes. We also study synergistic effects of a third metal in ternary $PtNi_3M$ (M = Co, Cu, Fe, Cr) cathode electrocatalysts. All catalyst precursor materials were prepared by an impregnation, freeze-drying, annealing route. After deployment of the catalyst precursor in single PEM cells, the active dealloyed form of the catalysts was obtained through a voltammetric dealloying protocol. Dealloyed binary PtM_3 catalysts showed more than a threefold activity improvement for ORR for M = Co, Cu, and close to a threefold improvement for M = Ni in terms of the Pt-mass activity ($A\,mg_{Pt}^{-1}$) of the single fuel cell, compared to a 45 wt% Pt/C reference cathode catalyst. Improvements in specific surface area normalized activities ($A\,cm_{Pt}^{-2}$) followed those in Pt-mass activity. All ternary catalysts, except the Fe containing one, showed clearly improved catalytic ORR performance compared to $PtNi_3$, in particular $PtNi_3Co$ and $PtNi_3Cu$. A previously unachieved four- to fivefold activity improvement in real single MEAs was observed.

Near-surface (XPS) and bulk (EDS/ICP) compositional characterizations suggested that the degree of dealloying of Pt–Co and Pt–Ni binary precursors is lower than that of Pt–Cu compounds. Pt–Co and Pt–Ni still showed 15–20 at.% non-noble metal near the surface and in the bulk of the dealloyed particles, whereas, under the chosen dealloying conditions, Pt–Cu formed core–shell structures with a Pt-rich surface and a Pt–Cu core. Of the selectively characterized Pt–Ni–Co and Pt–Ni–Cu ternaries, the near-surface composition of dealloyed Pt–Ni compounds showed an atomic ratio of about 1:1, compared to about 5:1 in the bulk, pointing to a Ni enrichment at the surface with only small residual amounts of Co or Cu.

Our study highlights a number of novel active cathode catalyst compositions and underscores the sensitive dependence of the ORR activity of dealloyed Pt binary and ternary nanoparticle electrocatalysts on the nature and initial composition of the non-noble alloy component.

1. Introduction

Hydrogen polymer electrode membrane fuel cells (PEMFCs) are a green alternative to fossil-fuel operated thermal combustion engines for powering vehicles, because the byproduct of hydrogen fuel cell power is simply water. A problem with using hydrogen fuel cells is their high cost, largely due to the use of the expensive element platinum on both the fuel cell anode and cathode. Large amounts of platinum, up to several grams of Pt/kW power out-

* Corresponding author at: The Electrochemical Energy, Catalysis, and Materials Science Laboratory, Department of Chemistry, Chemical Engineering Division, Technical University Berlin, 10623 Berlin, Germany. Tel.: +49 3031429542; fax: +49 3031429542.
E-mail address: pstrasser@tu-berlin.de (P. Strasser).

0378-7753/$ – see front matter © 2010 Elsevier B.V. All rights reserved.
doi:10.1016/j.jpowsour.2010.07.047

put, are required at the cathode of a hydrogen fuel cell in order to catalyze the sluggish electrocatalytic reduction of molecular oxygen molecules into electricity and water at a sufficiently high rate. The kinetics of the oxygen reduction reaction (ORR) is therefore currently a major barrier to more cost-efficient PEMFCs. The most active proven cathode ORR electrocatalyst is currently the nanostructured thin-film catalyst (NSTF) concept introduced a few years ago by 3M [1–3]. This catalyst concept does not rely on high surface area carbon supports. Instead, organic perylene whiskers offer support to sputtered extended Pt and Pt alloy films of Pt–Co, Pt–Mn–Co. Recently, 3M has extended their metal alloy catalyst of choice to a Pt-poor Pt–Ni [3]. NSTF catalyst have achieved some of the highest Pt-mass ($0.4\,A\,mg_{Pt}^{-1}$ for Pt_3Ni_7 at 900 mV) and specific activities ($2500\,\mu A\,cm_{Pt}^{-2}$ at 900 mV) ever observed in single MEAs under realistic conditions.

Dealloyed Pt nanoparticle electrocatalyst are a recently developed class of nano-structured alloy catalysts, which are highly active for ORR in acidic media [4–7]. Dealloying is the partial selective removal of a less noble alloy component from a bimetallic precursor [8–14]. In contrast to Pt-rich precursors, such as Pt_3M [15–20], Pt-poor precursors show massive removal of the less noble component from the bulk of the precursor materials associate with drastic rearrangement of Pt-surface and bulk atoms by surface diffusion. Hence, the electrochemical dissolution is not limited to the surface layer of the catalyst. Precursors include disordered alloys (solid solutions) or ordered alloys (intermetallic compound). Upon dealloying of the less noble (more active) component, the more noble alloy component is left behind under significant atomic rearrangement and loss of long range atomic order, accumulating near the catalytic interface the dealloyed material [21–25].

Dealloyed Pt–Cu nanoparticle electrocatalysts were studied intensively and showed Pt-mass-based as well as Pt-surface area-based ORR activity enhancements of 4–6× compared to pure Pt nanoparticles in both rotating disk electrode (RDE) set-ups [7] as well as single membrane electrode assembly (MEA) measurements [4–7]. At 900 mV/RHE, Pt-mass-based ORR activities ranged beyond $0.6\,A\,mg_{Pt}^{-1}$ and Pt-surface area-based ORR activities reached over $1000\,mA\,cm_{Pt}^{-2}$. The sixfold mass activity increase will allow the reduction of the Pt related cost at the cathode by more than 80%.

The mechanism of the catalytic enhancement of bulk-dealloyed particle catalysts is not based on roughening, that is, an increase in the real surface area of the catalytic interface, as is often found for Pt-rich bimetallic ORR catalysts [15]. The activity benefit of dealloyed Pt–Cu particles lies in the nanoscale structure of the dealloyed particles. Dealloyed Pt–Cu nanoparticles showed a core–shell structure after dealloying with a Pt-rich particle shell and a Pt–Cu alloy core [4]. The interatomic distance in the Pt-rich particle shell was found to be smaller than expected based on the chemical composition of the particle shell, which evidence the presence of compressive strain in the particle shell. This compressive strain was found to be a controlling factor of the ORR activity of dealloyed Pt–Cu particles. Durability studies of dealloyed Pt–Cu particles revealed superior Pt-mass-based activities after thousands of hours of operation compared to commercial pure Pt [12,26]. However, a disadvantage of dealloyed Pt–Cu alloy catalysts is that once Cu ions are leached into the fuel cell membrane they can reach the anode and subsequently electrodeposit there as metallic Cu film, based on its more positive corrosion potential compared to hydrogen. Based on that, less noble alloy components, such as Co, Ni, Fe, or Cr were hypothesized to offer advantages over Cu in terms of their medium and long-term Pt-mass-based and Pt-surface area-based performance at PEMFC cathodes.

Here, we test this hypothesis and present a comparative study of the PEMFC performance of dealloyed PtM_3 (M = Cu, Ni, Co) nanoparticle catalysts as well as dealloyed ternary $PtNi_3M$ (M = Cu, Co, Fe, Cr) catalysts in single fuel cells; precursor alloy materials were deployed in membrane electrode assemblies (MEAs) and subsequently dealloyed by voltammetric potential sweeps. The ternary compounds were selected based on the stability of Ni-based alloys and the similarity of the atomic radii of the used transition metals. The ternary study was designed to investigate synergistic effects of two non-noble transition metals for the ORR.

2. Experimental methods

2.1. Synthesis and characterization of Pt alloy precursors

PtM_3 and $PtNi_3M$ alloy precursors were prepared by an impregnation/freeze-drying route followed by annealing. Preparation started with impregnation of a commercial 30 wt% Pt/C catalyst (Tanaka Kikinzoku Kogyo International, Inc.) on high surface carbon with an aqueous solution of a metal nitrate(s) (Sigma–Aldrich, Inc.), followed by freezing in liquid N_2 [4,6,27]. The frozen sample was subsequently dried under a moderate vacuum (10^{-3} Torr). Pt and M were finally annealed under a reductive H_2 atmosphere using a Lindberg/Blue tube furnace. The bulk atomic composition of the catalysts was determined using a JEOL JSM6330F energy dispersive spectrometer (EDS) after calibrating with the respective pure metal standards. Alternatively, a VARIAN 820-MS inductively coupled plasma-mass spectrometer (ICP-MS) was utilized to determine bulk catalyst compositions. Surface atomic composition of the nanoparticles was performed by PHI Model 5700 X-ray photoelectron spectrometer (XPS). X-ray diffraction (XRD) analysis of the alloy precursor was performed by a Siemens D5000 diffractometer. The Cu Kα source was operating at a potential of 35 kV and a current of 30 mA.

2.2. Membrane electrode assembly (MEA) fabrication

Catalyst inks were prepared following procedures defined in earlier reports [6]. Inks were made by blending carbon-supported catalyst precursors with cold isopropyl alcohol (refrigerated for 15 min prior to use) followed by 5 min ultrasonication. A 5 wt% Nafion® solution was then added achieving a Catalyst:Nafion® dry weight ratio of 3:1, followed by additional sonication. Cathodes were composed of the synthesized Pt alloy precursor or a 45 wt% Pt/C commercial benchmark catalyst (TKK Inc.), while the anodes were made using commercial 40 wt% Pt/C (E-tek Inc.) throughout. MEAs were prepared by spraying these inks through an atomizing nozzle directly onto the 50 μm thick Nafion® NRE212 membrane using a high-precision robotic machine (PVA 350, PVA Inc.), followed by heat treatment (drying) at 80 °C for 24 h.

2.3. Single cell build, electrochemical dealloying and fuel cell testing

The prepared MEAs with active area of $10\,cm^2$ were then assembled into a single fuel cell using two gas diffusion media (GDL 10BC, Sigracet®, SGL Carbon Inc.) and three-channel serpentine flow field blocks (Poco® graphite blocks, supplied by Fuel Cell Technologies Inc.) equipped with gold-coated current collectors [6].

The Pt alloy cathode precursor materials were *electrochemically dealloyed* during a break-in humidification step followed by a potential sweep. First, the MEA was activated at 80 °C, 100% RH (H_2/O_2), $101.3\,kPa_{(abs)}$ with cell potential held constant at 0.6 V for 3 h. Then, the MEA conditions were changed to T(Cell) = 80 °C, 100% RH (H_2/N_2), $101.3\,kPa_{(abs)}$. Using a potentiostat (GAMRY Ref. 600) attached to the MEA, the cathode potential was cycled 200× at $100\,mV\,s^{-1}$ between 0.5 and 1.0 V vs RHE to dissolve non-noble metals from the surface of the cathode electrocatalysts. Thereafter, the MEA was disassembled and treated twice with 1 M H_2SO_4 at 80 °C for 1 h. After rinsing of the ion exchanged MEA with copious

amounts of deionized water, the MEA was re-assembled with a new gas diffusion media for fuel cell testing of the dealloyed catalyst layers.

For fuel cell testing, the relative humidity of the feed stream for anode and cathode was set at 100% for 80 °C cell temperature. The MEAs were activated with a 24 h potentiostatic hold at 0.6 V under 150 kPa_{abs} pressure before recording current-voltage characteristics at 150 kPa_{abs}. Polarization curves were taken using stoichiometric flows of $\lambda = 2/10$ (H_2/O_2) for $i \geq 0.2$ and 0.2 A cm^{-2} flows for $i < 0.2$ A cm^{-2}. The performance of the fuel cell was monitored by a data acquisition system from start to stop. IR correction was done by correcting the cell voltage with measured ohmic resistance of the fuel cell by an inbuilt AC impedance analyzer operating at 1 kHz frequency.

2.4. Electrochemical characterization after MEA testing

The H_2 crossover current in the MEA was determined at the end of the test protocol by linear sweep voltammetry (LSV) for T_{cell} = 80 °C, RH = 100%. The potential was swept at 2 mV s^{-1} from 0.05 to 0.6 V. At >0.4 V the resulting hydrogen oxidation current is purely limited by the H_2 permeation rate.

Cyclic voltammetry (CV) was applied between 0.05 and 1.2 V vs RHE (T_{cell} = 30 °C, RH = 100%, 20 mV s^{-1}) in order to measure the electrochemical Pt-surface area ($ECSA_{Pt}$) of the cathode electrocatalysts. The charge for monolayer hydrogen adsorption/desorption was assumed to be 210 μC cm_{Pt}^{-2}. For the CV and the LSV characterizations, the H_2 anode served as a counter and reference electrode and the N_2-purged cathode was the working electrode, with gas flows of H_2/N_2 = 160 mL min^{-1}. All the voltages of CV and LSV experiments are reported relative to the reversible hydrogen electrode (RHE).

3. Results and discussion

3.1. Structural characterization of PtM_3 and $PtNi_3M$ catalyst precursors

Fig. 1 displays the X-ray diffraction pattern of $PtCo_3$, $PtNi_3$ and $PtCu_3$ alloy precursors annealed at 600 °C for 7 h. The profiles suggest the formation of disordered face centered cubic solid solutions of Pt and Cu, Co, and Ni. The (1 1 1) fundamental reflections of the three alloys fall between the values of pure Pt 39.8°

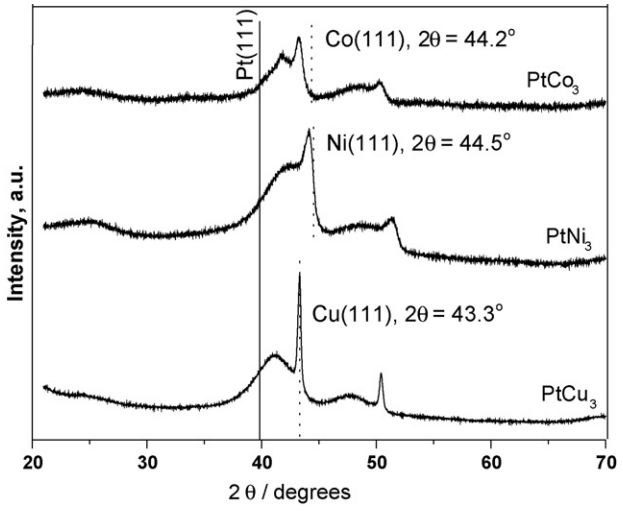

Fig. 1. X-ray diffraction patterns of carbon-supported binary PtM_3 (M = Co, Ni, Cu) nanoparticle catalyst precursors. The fundamental (1 1 1) reflection of face centered cubic Pt, Cu, Ni, and Co are indicated by vertical lines.

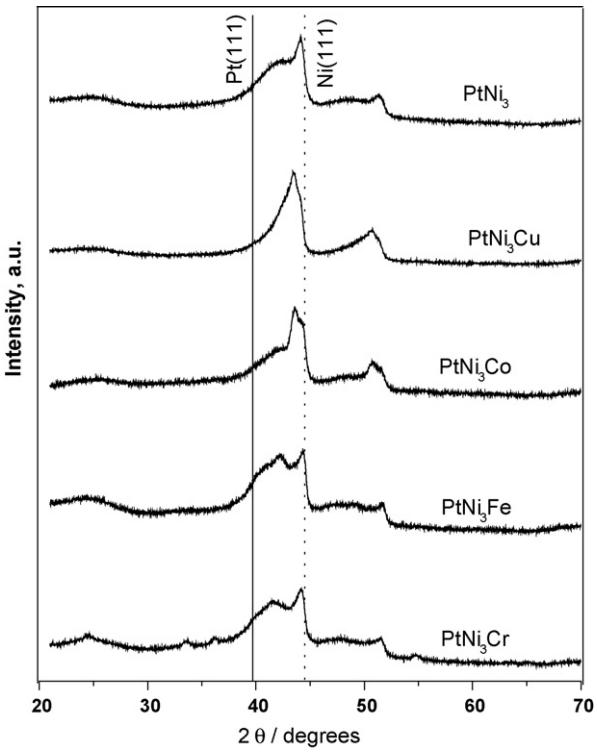

Fig. 2. X-ray diffraction patterns of carbon-supported ternary $PtNi_3M$ (M = Co, Cu, Fe, Cr) nanoparticle catalyst precursors. The fundamental (1 1 1) reflection of face centered cubic Pt and Ni are indicated by vertical lines.

(solid vertical line) and those 2θ values of the pure base metals [28]. This reflects a reduced lattice parameter by the incorporation of smaller metal atoms into the Pt lattice. In addition to the solid solution alloy peaks, $PtCu_3$ precursor shows the presence of large pure Cu crystallites ((1 1 1) reflection of pure Cu at 43.3°), whereas $PtCo_3$ and $PtNi_3$ shows the existence of at least one other Co and Ni-rich crystalline alloy phase, evidenced by (1 1 1) reflections just left of those of pure Co (44.4°) and Ni (44.5°). Fig. 2 shows the diffraction profiles of the ternary $PtNi_3Co$, $PtNi_3Cu$, $PtNi_3Fe$ and $PtNi_3Cr$ catalyst precursor alloys. All ternaries show complex multiphase alloy structures with one sharp reflection near the pure Ni (1 1 1) position indicating large Ni-rich crystallites and at least one Pt-rich alloy phase. There is no indication of superlattice peaks at smaller 2θ values and hence of ordered intermetallics. $PtNi_3Cr$ exhibited weak reflections characteristic for chromium oxide.

3.2. Voltammetric dealloying of Pt alloy precursor cathode

Fig. 3 shows three cyclic voltammetric profiles of the as-prepared and dealloyed catalyst inside the MEA. The solid trace represents the initial dealloying CV of the MEA cathode containing the freshly prepared $PtCu_3$ precursor material. Initially, the electrode potential was scanned anodically from 0.05 to 1.2 V and back. Around 0.37 V vs RHE the electrochemical dissolution of pure Cu crystallites as well as Cu surface atoms in a predominantly Cu environment can be discerned. As observed in previous studies, there is no indication of the characteristic H desorption peak in the so-called H_{upd} region (0.05–0.4 V/RHE). At more positive electrode potentials, an anodic voltammetric waves around 0.7 V can be attributed to the dissolution of Cu atoms coordinated predominantly by Pt atoms. This is similar to the dissolution of underpotentially deposited Cu atoms on pure Pt surfaces. At electrode potentials of 0.8 V and higher, anodic voltammetric waves

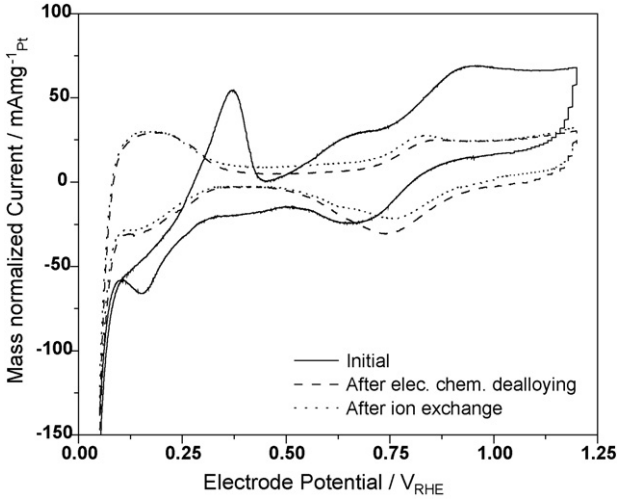

Fig. 3. Cyclic voltammetric profiles of a single MEA prepared using a $PtCu_3$ alloy cathode catalysts measured during the first scan of in situ dealloying (solid), after dealloying (dashed) and after ion exchange (dotted).

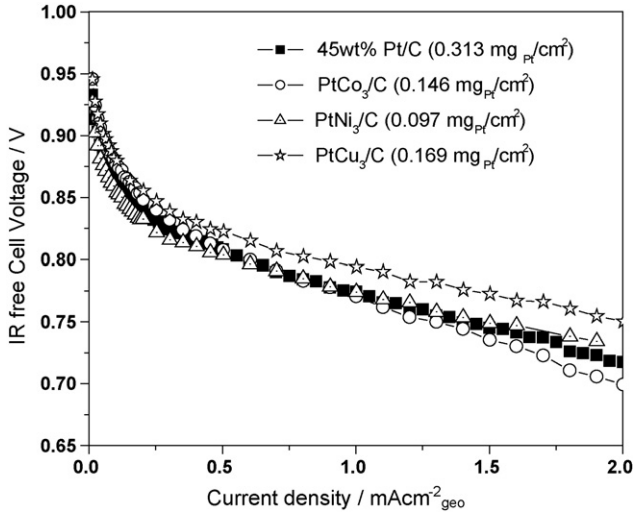

Fig. 4. *V–I* characteristics (polarization curve) of single cell MEAs prepared using carbon-supported $PtCo_3$, $PtNi_3$, and $PtCu_3$ alloy precursors on the cathode. The *V–I* curves were measured after in situ voltammetric dealloying of the cathode catalysts. Conditions: 80 °C, 100% RH, H_2/O_2, 10 cm^2 area, geometric Pt loadings are given in parentheses.

indicate the formation of oxygenated surface species, such as Pt–OH and Pt–O, and Pt-surface oxides in agreement with previous reports. In the reverse cathodic scan, the desorption of the oxygenated species appears at around 0.65 V, while some Cu^{2+} deposition may occur at around 0.3 V. After recording the initial voltammetric response, the cathode is continuously electrochemically dealloyed by continued potential cycling between 0.5 and 1.0 V/RHE to strip away any pure Cu phase and dealloy the Cu-rich Pt alloy phases. The lower turning potential of 0.5 V was chosen in order to stay well above the onset of Cu reduction potential and hence to avoid any Cu plating. The course of the dealloying process was continued until a time stable CV profile was obtained. During this process, the base metal rich surface is gradually electrochemically dealloyed (selective dissolution of Cu atoms) leaving a Pt-enriched catalyst surface behind. Full range (0.05–1.2 V) cyclic voltammograms (not shown) taken at regular intervals during the dealloyed process revealed the emergence of the typical underpotential ad/desorption of hydrogen atoms on the dealloyed Pt-enriched catalyst. The voltammogram taken at the end of the dealloying process resembles that of pure Pt (Fig. 3, dashed line). Finally, after the dealloying process the MEA was disassembled and ion exchanged with a mineral acid in order to remove any residual Cu^{2+} ions in the ionomer of the catalyst layer (see Section 2.3). After reassembly of the MEA, the cathode catalyst shows a subtle improvement in interfacial capacity (Fig. 3, dotted line), however, the CV shows that the basic Pt like surface features of the dealloyed catalysts remained after ion exchange. An identical procedure was used for all other alloy precursor materials, however, due to the negative oxidation potential of $Ni^0 \rightarrow Ni^{2+}$ [−0.25 V], $Co^0 \rightarrow Co^{2+}$ [−0.28 V], $Fe^0 \rightarrow Fe^{2+}$ [−0.44 V] and $Cr^0 \rightarrow Cr^{3+}$ [−0.74 V] we were not able to monitor the oxidative/reductive current for these non-Pt alloy components directly. After ion exchanging, the MEA is free of metal cations and ready for further testing.

3.3. Activity of the electrochemically dealloyed PtM_3 nanoparticles

Performance testing of electrochemically dealloyed Pt–M alloy cathodes were carried out at 80 °C, 100% RH, and 150 kPa_{abs} (i.e. reactant gas pressures close to the reference pressure of 101 kPa_{abs}) with pure (99.99%) H_2 and O_2. These are standard conditions recommended recently by leading fuel cell developers [29]. Fig. 4 illustrates that MEAs with dealloyed Pt cathodes show comparable or improved current densities over a broad current density range despite their drastically reduced geometric Pt loadings (0.1–0.17 mg_{Pt} cm^{-2} for Pt–M vs 0.3 mg_{Pt} cm^{-2} for Pt). In particular, Fig. 4 shows that the dealloyed catalysts do not cause detrimental effects in the ohmic and mass transport region of the polarization curve. To contrast the kinetic activity of dealloyed Pt catalysts against that of commercial pure Pt cathode catalysts, the kinetic current density of the single cell measurements of Fig. 4 was normalized with respect to both the Pt loading of the electrode, yielding mass activity values (Fig. 5a) and the real Pt-based ECSA, resulting in values of the specific activity (Fig. 5b). $PtCo_3$ and $PtCu_3$ are clearly more active that $PtNi_3$, as is evident by their 3–4× enhancement in mass *and* specific activity, compared to the commercial "state-of-the-art" 45 wt% Pt/C catalyst. The absolute values for the activities for the electrochemically dealloyed MEA cathodes at 0.9 V (IR corrected) are summarized in Table 1. The $ECSA_{Pt}$ values of Pt–Co and Pt–Cu were about 70 m^2 g^{-1}, comparable to 45 wt% Pt/C, that of

Table 1
Characteristics of carbon-supported binary PtM_3 (M = Co, Ni, Cu) nanoparticle fuel cell cathode electrocatalysts: selected bulk and near-surface compositional of as-prepared alloy precursors and final electrocatalysts after dealloying, electrochemically active surface area after dealloying (ECSA), and electrocatalytic performance. The standard Pt material is a commercially available 45 wt% carbon-supported Pt catalyst.

Nominal composition	EDS composition (as prepared) [at.%]	XPS composition (as prepared) [at.%]	ICP composition (after dealloying) [at.%]	XPS composition (after dealloying) [at.%]	$ECSA_{Pt}$ [m^2 g_{Pt}^{-1}]	Mass activity @ 0.9 V [A mg_{Pt}^{-1}]	Specific activity @ 0.9 V [μA cm_{Pt}^{-2}]
Pt	–	–	–	–	63	0.104	166
$Pt_{25}Co_{75}$	$Pt_{26}Co_{74}$	$Pt_{42}Co_{58}$	$Pt_{83}Co_{17}$	$Pt_{86}Co_{14}$	70	0.346	491
$Pt_{25}Ni_{75}$	$Pt_{18}Ni_{82}$	$Pt_{38}Ni_{62}$	$Pt_{82}Ni_{18}$	$Pt_{77}Ni_{23}$	111	0.275	248
$Pt_{25}Cu_{75}$	$Pt_{35}Cu_{65}$		$Pt_{87}Cu_{13}$	$Pt_{98}Cu_2$	72	0.340	472

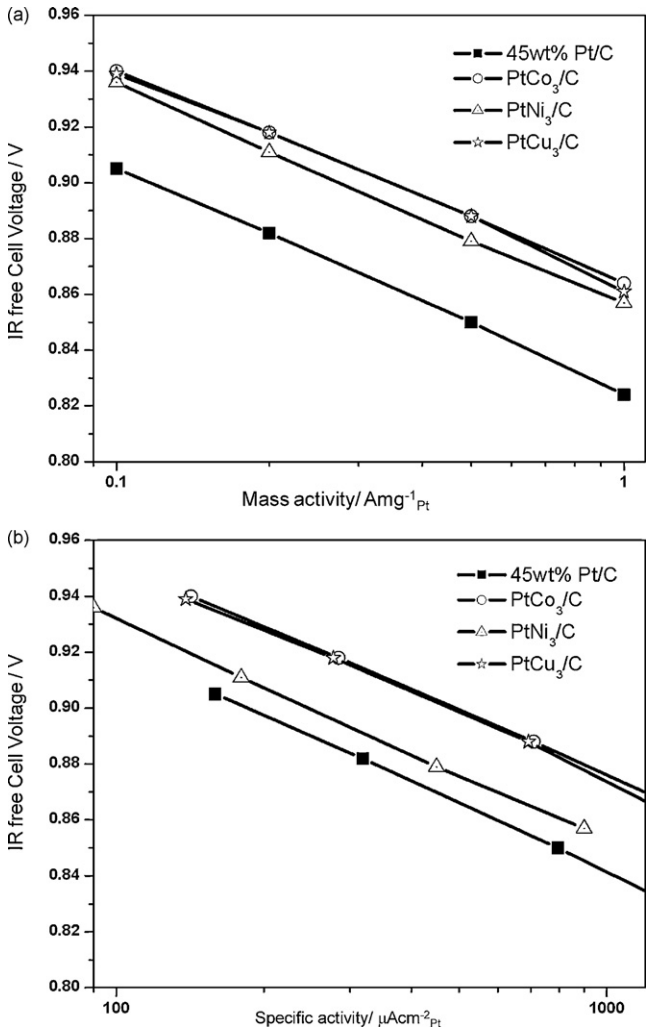

Fig. 5. Tafel plots derived from *V–I* curves in Fig. 4 comparing the catalytic performance of dealloyed $PtCo_3$, $PtNi_3$, and $PtCu_3$ cathodes with a standard Pt cathode. (a) Pt-mass activity ($A\,mg_{Pt}^{-1}$) and (b) specific activity ($\mu A\,cm_{Pt}^{-2}$).

Pt–Ni was about 50% higher indicating a higher degree of roughening of the dealloyed Pt–Ni surface compared that of Co or Cu. Note that specific activities are normalized to the ECSA values; hence, the Pt–Ni catalyst showed a 3× increase in specific activity despite the higher $ECSA_{Pt}$. The Pt-mass-based activities of single fuel cells reported in Table 1 range among the highest activities ever reported for single PEMFC under realistic conditions.

The atomic compositions of the as-prepared PtM_3 alloys determined by EDS analysis were close to the nominal values with Pt being between 20 and 30 at.% (see Table 1, column 2), while the near-surface composition of selected precursors was around 40 at.% Pt, hence slightly Pt-enriched compared to the bulk (see Table 1, column 3). After electrochemical dealloying the composition of the base metal atoms on the surface and in the bulk was drastically reduced (see Table 1, columns 4 and 5). The overall base metal content in the bulk and at the surface for the Pt–Co and Pt–Ni was now around 15–20 at.%. Pt–Cu showed a highly depleted Cu content near the surface compared to the bulk, in line with a reduced Pt-surface segregation tendency in Pt–Cu bimetallic alloys [30–33]. Cu bulk atoms appear to leach more readily and to a larger extent from Cu-rich alloy nanoparticles compared to Ni or Co alloys, in line with Pt–Ni and Pt–Co showing a preference of Pt atom segregation to the surface, thereby slowing down the extent and possibly rate of bulk Co and Ni.

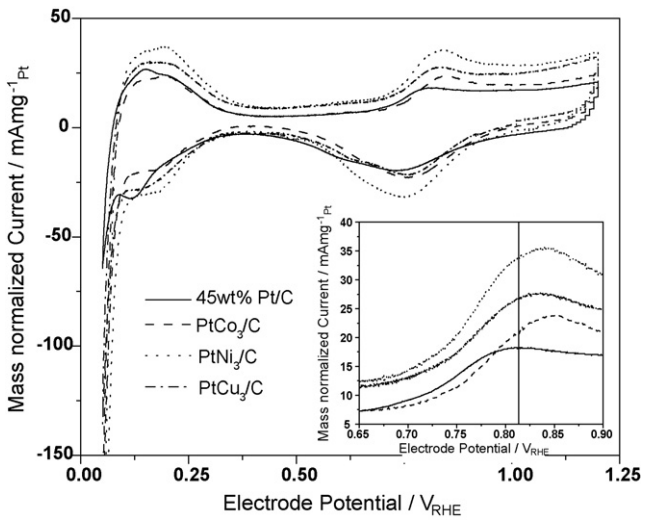

Fig. 6. Cyclic voltammetric profile of dealloyed $PtCo_3$, $PtNi_3$, and $PtCu_3$ cathodes. Scan rate was 20 mV/s. Inset shows significant anodic shift of the voltammetric wave associated with water activation/surface OH formation when dealloyed binary cathode electrocatalysts were utilized. Standard Pt cathode catalysts are shown for comparison.

Fig. 6 compares and contrasts the cyclic voltammetric profiles of the individual PtM_3 cathode electrocatalysts after performance testing, with the Pt-mass-normalized current density plotted at the *y* axis. The relative ECSA values represented by the integral charges in the *H*(upd) region, 0.05–0.4 V/RHE follow the measured trends prior to performance testing (Table 1, column 6). The inset shows a blow up of the water activation/M–OH formation region on the anodic scans. For all the electrochemically activated Pt–M catalyst Fig. 6 reveals a distinct anodic shift in the peak electrode potential of the voltammetric wave associated with the water activation/surface OH formation. Compared to the pure Pt catalyst, peak potential shifts range up to 50 mV. This shift has been associated with a weakened interaction between oxygenated surface species, such as O and OH, and the dealloyed Pt-surface; the shift is a common feature of improved ORR catalysts [34]. Also, the voltammetric charge associated with the anodic peak current densities of the surface M–OH and M–O formation, especially that for $PtNi_3$ and $PtCu_3$, were higher than that for Pt reflecting the trends in ECSA.

3.4. Activity of the electrochemically dealloyed $PtNi_3M$ nanoparticles

Large ECSA values of dealloyed $PtNi_3$ cathode catalyst combined with the voltammetric stability of Ni alloys in acidic and alkaline solutions [35,36] make these materials ideal for further optimization of ORR performance. On the other hand, Pt–Cu alloys were found to dissolve to a larger extent than Pt–Co or Pt–Ni introducing favorable Pt enrichment for ORR (see Table 1). Clearly, the combination of both features, stability and high activity is desired and hence ternary dealloyed $PtNi_3M$ materials with M = Cu, Co, Fe, and Cr were prepared and in situ dealloyed inside MEAs and subsequently tested for performance and catalytic activity.

The performance of the electrochemically dealloyed $PtNi_3M$ ternaries were compared with $PtNi_3$ binary and state-of-the-art commercial 45 wt% Pt/C catalysts. From Fig. 7, it is apparent that $PtNi_3Co$ and $PtNi_3Cu$ outperform commercial 45 wt% Pt/C catalysts, whereas $PtNi_3Fe$ and $PtNi_3Cr$ show comparable performance even with only 1/3 of geometric Pt loading of the commercial catalysts. No mass transport limitations were discernible over the entire current density range. On comparing the mass and specific activities (Fig. 8a, b and Table 2) in the kinetic region, there is clear

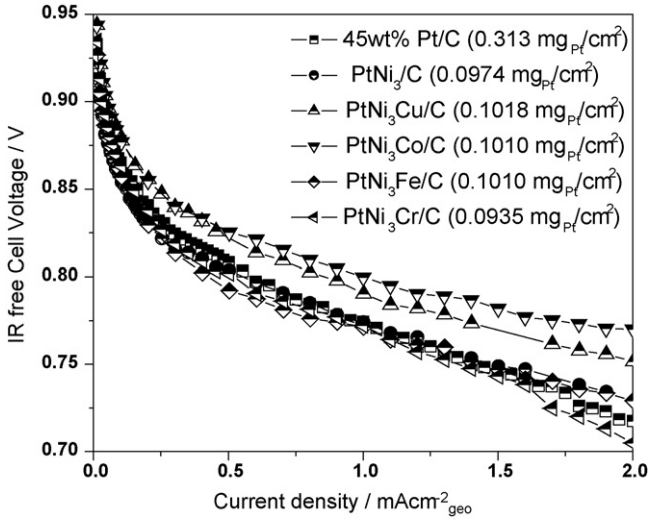

Fig. 7. *V–I* characteristics (polarization curve) of single cell MEAs prepared using $PtNi_3M$ (M = Co, Cu, Fe, Cr) alloy precursors on the cathode. The *V–I* curves were measured after in situ voltammetric dealloying of the cathodes. Conditions: 80 °C, 100% RH, H_2/O_2, 10 cm^2 area, geometric Pt loadings are given in parentheses.

synergy between the Pt–Ni bimetallic alloy and additional third alloying components. The largest activity advantage over $PtNi_3$ was observed for $PtNi_3Co$ and $PtNi_3Cu$ ternaries with a Pt-mass activity improvement of 1.7× over $PtNi_3$. $PtNi_3Cr$ still showed 1.3× improvement and $PtNi_3Fe$ showed negligible advantage in mass activity over the Pt–Ni compounds. Synergistic effects of combining Co, Cu or Cr with the $PtNi_3$ amounted to previously unobserved and unprecedented Pt-mass activity improvements of a factor of 5× for $PtNi_3Co$ and $PtNi_3Cu$ and 3.5× for $PtNi_3Cr$ compared to pure Pt (see Table 2). Similar to the binary compounds, a 50–60 mV anodic shift of the Pt–OH formation was evident for all dealloyed ternary compounds at the end of the performance tests (Fig. 9).

To better correlate activity enhancements of the ternary catalysts with atomic scale compositional changes during dealloying and testing, bulk and near-surface characterization of the catalysts before and after dealloying was performed. The bulk atomic compositions of most of the as-prepared $PtNi_3M$ ternaries were close to the nominal compositions. XPS analysis shows the atomic composition of Pt at the surface of the as-prepared alloy precursors analyzed was about 40 at.% Pt irrespective of the detailed nature of the alloying components. The 40:40:20 atomic ratio of the Pt:Ni:Co or Pt:Ni:Cu suggests some Pt segregation to the surface of the annealed precursors in accordance with predictions of the surface segregation behavior of Pt [33]. After electrochemical dealloying and performance testing the bulk and surface atomic composition of Pt clearly increased in all catalysts, as expected, due to surface and bulk dealloying of the less noble metals.

Pt bulk compositions rose to 75–86 at.% in accordance with results from the binary compounds, the remainder being split

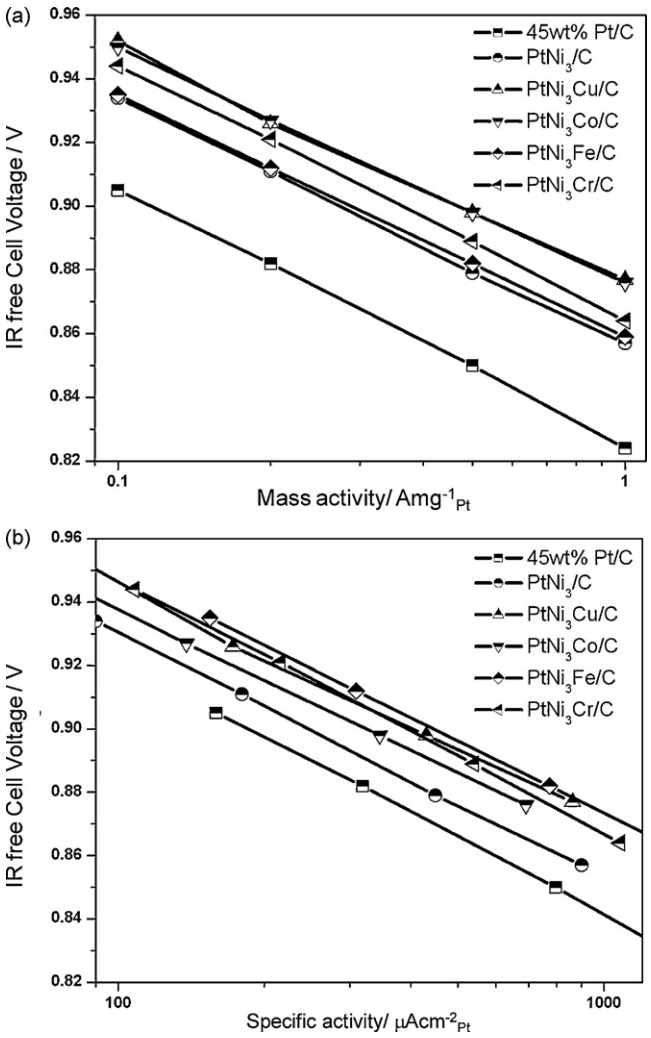

Fig. 8. Tafel Plots derived from *V–I* curves in Fig. 7 comparing the catalytic performance of dealloyed $PtNi_3M$ (M = Co, Cu, Fe, Cr) cathodes with a standard Pt cathode. (a) Pt-mass activity (A mg_{Pt}^{-1}) and (b) specific activity (μA cm_{Pt}^{-2}).

between Ni and the third non-noble metal. The most active dealloyed catalysts, Pt–Ni–Co and Pt–Ni–Cu ternaries retained very small amounts of Cu and Co in the bulk. Dealloyed Pt–Ni–Cr showed higher final content in Cr (22 at.% in bulk) than in Ni (3 at.%), underlining the corrosion resistance of Cr due to oxide formation possibly accelerating the dissolution of Ni surface atoms. Near-surface XPS compositional analysis of the ternary cathode catalysts after electrochemical dealloying revealed a very similar surface at.% value for Pt as for Ni, typically around 48–49 at.% for the sample investigated. Hence, their relative surface composition ratio remained stable near 1:1 before and after dealloying; this underscores the

Table 2
Characteristics of carbon-supported ternary $PtNi_3M$ (M = Co, Cu, Fe, Cr) nanoparticle fuel cell cathode electrocatalysts: Selected bulk and near-surface compositional of as-prepared alloy precursors and final electrocatalysts after dealloying, electrochemically active surface area after dealloying (ECSA), and electrocatalytic performance. The standard Pt material is a commercially available 45 wt% carbon-supported Pt catalyst.

Nominal composition	EDS composition (as prepared) [at.%]	XPS composition (as prepared) [at.%]	ICP composition (after dealloying) [at.%]	XPS composition (after dealloying) [at.%]	$ECSA_{Pt}$ [m^2 g_{Pt}^{-1}]	Mass activity @ 0.9 V [A mg_{Pt}^{-1}]	Specific activity @ 0.9 V [μA cm_{Pt}^{-2}]
Pt	–	–	–	–	63	0.104	166
$Pt_{25}Ni_{75}$	$Pt_{18}Ni_{82}$	$Pt_{38}Ni_{62}$	$Pt_{82}Ni_{18}$	$Pt_{77}Ni_{23}$	111	0.275	248
$Pt_{20}Ni_{60}Cu_{20}$	$Pt_{19}Ni_{56}Cu_{25}$	$Pt_{38}Ni_{40}Cu_{22}$	$Pt_{82}Ni_{15}Cu_3$	$Pt_{48}Ni_{48}Cu_4$	116	0.473	406
$Pt_{20}Ni_{60}Co_{20}$	$Pt_{14}Ni_{65}Co_{21}$	$Pt_{41}Ni_{37}Co_{22}$	$Pt_{86}Ni_{11}Co_3$	$Pt_{45}Ni_{49}Co_6$	145	0.472	326
$Pt_{20}Ni_{60}Fe_{20}$	$Pt_{20}Ni_{60}Fe_{20}$	–	–	–	65	0.289	447
$Pt_{20}Ni_{60}Cr_{20}$	$Pt_{14}Ni_{49}Cr_{37}$	–	$Pt_{75}Ni_3Cr_{22}$	–	92	0.366	396

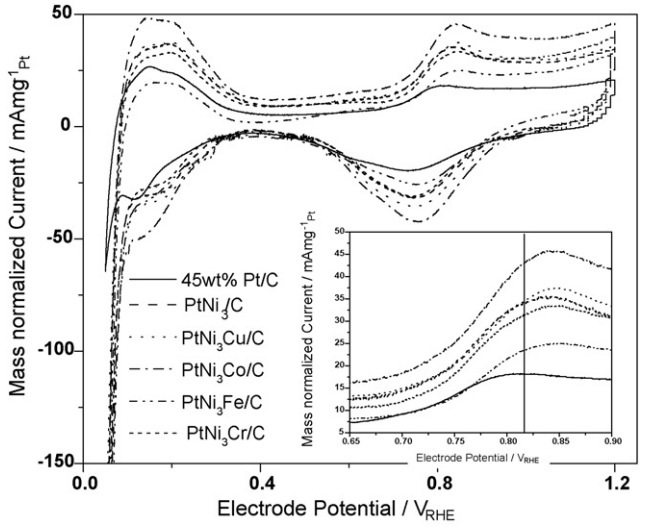

Fig. 9. Cyclic voltammetric profile of dealloyed $PtNi_3M$ (M = Co, Cu, Fe, Cr) cathodes. Scan rate was 20 mV/s. Inset shows significant anodic shift of the voltammetric wave associated with water activation/surface OH formation when dealloyed binary cathode electrocatalysts were utilized. Standard Pt cathode catalysts are shown for comparison.

stability of Pt and Ni in ternary alloys, and highlights the "sacrificial nature" of the Co or Cu alloy components in the ternary catalysts. Dealloying reduced primarily the Co and Cu content of the catalyst resulting in a final near-surface composition of only 4–6 at.%. The benefits of adding Co and Cu in the dealloyed catalysts are reflected in the resulting ECSA values of the Pt–Ni–Cu and Pt–Ni–Co catalysts. As Table 2 shows, the third metals further enhance the resulting ECSA, but at the same time enhance the ECSA normalized specific activity values. This means that the dealloyed Pt–Ni–M (M = Cu, Co) catalyst surface is in fact rougher than that of the Pt–Ni binary catalyst. However, roughening cannot explain the 3–6× improvement of the specific activity enhancement which accounts for the changes of the ECSA. A more favorable arrangement of the resulting Pt–Ni surface layer, possibly compressive surface strain combined with ligand effects between Ni and Pt are likely to shift chemisorption energies of the ORR intermediates into the direction of reduced overpotentials [4,18,37–39]. The ECSA values of the Cr and Fe containing compounds after dealloying (Table 2) are comparable to the pure Pt cathode catalyst reflecting the corrosion stability of Cr and Fe additions and reduced roughening of the interface. The specific activity of the Fe containing compound was found highest, while its Pt-mass activity was comparably poor.

4. Conclusions

Dealloyed Pt alloy nanoparticles are a highly promising class of electrocatalysts for the electroreduction of molecular oxygen at cathodes of PEMFC. In particular, dealloyed $PtCu_3$ catalysts have shown unprecedented ORR activities in rotating disk electrode (RDE) measurements [4,7,8].

Here we have extended and generalized the study of dealloyed Pt nanoparticle electrocatalysts demonstrating that dealloying of PtM_3 and $PtNi_3M$ nanoparticles result in catalyst materials with significantly improved activity compared to commercial pure Pt catalysts. Specifically, we have shown that PtM_3 (M = Cu, Co, Ni) bimetallic and $PtNi_3M$ (M = Cu, Co, Fe, Cr) ternary nanoparticle alloy electrocatalysts offer previously unachieved Pt-mass-based as well as Pt-surface area (specific) activities for the electroreduction of molecular oxygen in fuel cell gas diffusion electrodes.

Co and Cu containing dealloyed binary and ternary catalysts showed drastic dissolution of these metals after dealloying; based on their comparable ORR activities it is reasonable to assume that Cu and Co play similar functional roles in the formation of the final active catalytic interface. We suspect that, similar to Cu [4], the selective dissolution of Co creates a Pt-rich surface with geometric and chemisorption characteristics, which are more favorable for the ORR.

Due to their corrosion stability, the origin of the improved ORR activity of dealloyed $PtNi_3$ is not fully understood. Clearly, in the case of dealloyed Pt–Ni compounds the surface contains significant amounts of Ni atoms (Table 1). However, the current study shows that functional roles, such as stability of Ni, can be synergistically combined with activity enhancing alloy components, such as readily dissolving Cu and Co atoms resulting in overall improved electrocatalysts.

The MEA performance and ORR activity of dealloyed Pt nanoparticle cathode electrocatalysts is currently only rivaled by nano-structured-thin-film (NSTF) cathode catalysts developed by 3M Corporation. In particular, NSTF ORR activities [3] of a Pt_3Ni_7 alloy NSTF catalysts were reported to be as high as 0.4 A mg^{-1}_{Pt} and 2500 μA cm^{-2}_{Pt} at 900 mV cell voltage. We suspect that the origin of this ORR activity is in parts based in a partial bulk dealloying of the Ni alloy component from the catalyst film resulting in a catalytically active Pt-enriched dealloyed film structure. We want to point out that electrochemical surface area (ECSA) gains after dealloying of alloy thin films are typically much more pronounced (factor 50 and higher) than those for nanoparticles. Hence, ECSA gains play a more important role in the enhancement of dealloyed thin films.

Our study underscores the viability of dealloyed Pt electrocatalysts in H_2/O_2 operated PEMFCs under realistic conditions; it also highlights previous conclusions that dealloyed Pt catalysts are currently the most active nanoparticle fuel cell cathode catalyst concept [40].

Acknowledgements

This project was supported by the Department of Energy, Office of Basic Energy Sciences under the auspices of the President's Hydrogen Fuel Initiative. Acknowledgment is also made to the National Science Foundation (grant #729722) for partial support of this research. P.S. acknowledges financial support from the German National Science Foundation (DFG)-funded Center of Excellence in Catalysis (UNICAT) managed by the Technical University Berlin, Germany.

References

[1] M. Debe, in: W. Vielstich, A. Lamm, H.A. Gasteiger (Eds.), Handbook of Fuel Cells—Fundamentals, Technology, and Applications, vol. 3, John Wiley and Sons, 2003, p. 576.
[2] M.K. Debe, A.K. Schmoeckel, G.D. Vernstrom, R. Atanasoski, J. Power Sources 161 (2006) 1002.
[3] R. Atanasoski, M. Debe, Ulm Electrochemical Talks—"2015" Technologies on Batteries and Fuel Cells, Ulm, Germany, June 15–17, 2010.
[4] P. Strasser, S. Koh, T. Anniyev, J. Greeley, K. More, C. Yu, Z. Liu, S. Kaya, D. Nordlund, H. Ogasawara, M.F. Toney, A. Nilsson, Nat. Chem. 2 (2010) 454.
[5] R. Srivastava, P. Mani, N. Hahn, P. Strasser, Angew. Chem. Int. Ed. 46 (2007) 8988.
[6] P. Mani, R. Srivastava, P. Strasser, ECS Trans. 11 (2007) 933.
[7] S. Koh, P. Strasser, J. Am. Chem. Soc. 129 (2007) 12624.
[8] P. Strasser, Rev. Chem. Eng. 25 (2009) 255.
[9] P. Strasser, Chem. Ing. Tech. 81 (2009) 573.
[10] P. Strasser, Dealloyed Pt bimetallic electrocatalysts for oxygen reduction, in: W. Vielstich, H.A. Gasteiger, H. Yokokawa (Eds.), Handbook of Fuel Cells: Advances in Electrocatalysis, Materials, Diagnostics and Durability, vols. 5 and 6, John Wiley & Sons Ltd, Chichester, West Sussex, UK, 2009, p. 30.
[11] R. Srivastava, P. Mani, P. Strasser, J. Power Sources 190 (2009) 40.
[12] K.C. Neyerlin, R. Srivastava, C. Yu, P. Strasser, J. Power Sources 186 (2009) 261.
[13] P. Strasser, S. Koh, J. Greeley, Phys. Chem. Chem. Phys. 10 (2008) 3670.

[14] F. Fechner, P. Strasser, M. Eiswirth, F.W. Schneider, A.F. Munster, Chem. Phys. Lett. 313 (1999) 205.
[15] M.T. Paffet, J.G. Beery, S. Gottesfeld, J. Electrochem. Soc. 135 (1988) 1431.
[16] U.A. Paulus, A. Wokaun, G.G. Scherer, T.J. Schmidt, V. Stamenkovic, N.M. Markovic, P.N. Ross, Electrochim. Acta 47 (2002) 3787.
[17] U.A. Paulus, A. Wokaun, G.G. Scherer, T.J. Schmidt, V. Stamenkovic, V. Radmilovic, N.M. Markovic, P.N. Ross, J. Phys. Chem. B 106 (2002)4181.
[18] V. Stamenkovic, B.S. Moon, K.J. Mayerhofer, P.N. Ross, N. Markovic, J. Rossmeisl, J. Greeley, J.K. Norskov, Angew. Chem. Int. Ed. 45 (2006) 2897.
[19] V. Stamenkovic, B.S. Mun, M. Arenz, K.J.J. Mayerhofer, C.A. Lucas, G. Wang, P.N. Ross, N. Markovic, Nat. Mater. 6 (2007) 241.
[20] T. Toda, H. Igarashi, H. Uchida, M. Watanabe, J. Electrochem. Soc. 146 (1999) 3751.
[21] J. Erlebacher, M.J. Aziz, A. Karma, N. Dimitrov, K. Sieradzki, Nature 410 (2001) 450.
[22] K. Sieradzki, N. Dimitrov, D. Movrin, C. McChall, N. Vasijevic, J. Erlebacher, J. Electrochem. Soc. 149 (2002) B370.
[23] Y. Ding, M. Chen, J. Erlebacher, J. Am. Chem. Soc. 126 (2004) 6876.
[24] J. Erlebacher, J. Electrochem. Soc. 151 (2004) C614.
[25] J. Rugolo, J. Erlebacher, K. Sieradzki, Nature 5 (2006) 946.
[26] K.C. Neyerlin, R. Srivastava, P. Strasser, ECS Trans. 16 (2008) 509.
[27] S. Koh, N. Hahn, C. Yu, P. Strasser, J. Electrochem. Soc. 155 (2008) B1281.
[28] ICDD, International Center for Diffraction Data—Power Diffraction File (PDF) 2 Data CD, 2002, http://www.icdd.com/.
[29] H.A. Gasteiger, S.S. Kocha, B. Sompalli, F.T. Wagner, Appl. Catal. B: Environ. 56 (2005) 9.
[30] B. Hammer, Y. Morikawa, J.K. Nørskov, Phys. Rev. Lett. 76 (1996) 2141.
[31] B. Hammer, J.K. Nørskov, Surf. Sci. 343 (1995) 211.
[32] B. Hammer, J.K. Nørskov, in: R.M. Lambert, G. Pacchioni (Eds.), Chemisorption and Reactivity on Supported Clusters and Thin Films, Kluwer Academic Publishers, Netherlands, 1997, p. 285.
[33] A.V. Ruban, H.L. Skriver, J.K. Nørskov, Phys. Rev. B 59 (1999) 15990.
[34] V.R. Stamenkovic, B. Fowler, B.S. Mun, G. Wang, P.N. Ross, C.A. Lucas, N.M. Markovic, Science 315 (2007) 493.
[35] A.K.N. Reddy, B. Rao, Can. J. Chem. 47 (1969) 2693.
[36] M. Pourbaix, Atlas of Electrochemical Equilibria in Aqueous Solutions, Pergamon Press, Oxford, New York, 1966.
[37] J. Rossmeisl, J.K. Norskov, C.D. Taylor, M.J. Janik, M. Neurock, J. Phys. Chem. B 110 (2006) 21833.
[38] J. Greeley, J.K. Norskov, Surf. Sci. 592 (2005) 104.
[39] J.K. Norskov, J. Rossmeisl, A. Logadottir, L. Lindqvist, J.R. Kitchin, T. Bligaard, H. Jonsson, J. Phys. Chem. B 108 (2004) 17886.
[40] H.A. Gasteiger, N.M. Markovic, Science 324 (2009) 48.